International Journal of Minerals, Metallurgy and Materials
Volume 27, Number 9, September 2020, Page 1269
https://doi.org/10.1007/s12613-020-2020-5

Protein adsorption, cell viability and corrosion properties of Ti6Al4V alloy treated by plasma oxidation and anodic oxidation

Özgü Bayrak[1)], *Hojjat Ghahramanzadeh Asl*[2)], *and Ayşe Ak*[3)]

1) Department of Mechanical Engineering, Erzincan Binali Yıldırım University, Erzincan 24100, Turkey
2) Department of Mechanical Engineering, Karadeniz Technical University, Trabzon 61080, Turkey
3) Vocational School of Health Services, Medical Imaging Techniques Programme, Kocaeli University, Kocaeli 41001, Turkey
(Received: 23 November 2019; revised: 14 February 2020; accepted: 16 February 2020)

Abstract: The hardness, wettability, and electrochemical properties of Ti6Al4V alloy surfaces treated with anodic oxidation and plasma oxidation as well as the viabilities of the different cell lines on the obtained surfaces were investigated. The anodic oxidation was performed for 10 min under 100 V potential, and it resulted in a 0.95 μm thick nanoporous anatase-TiO_2 structure. On the other hand, plasma oxidation was carried out at 650°C for 1 h and resulted in a dense rutile-TiO_2 structure with a thickness of 1.2 μm. While a hardness of $HV_{0.025}$ 823 and roughness of ~220 nm were obtained by plasma oxidation, those obtained by anodic oxidation were $HV_{0.025}$ 512 and ~130 nm, respectively. The anodic oxidation process created a more hydrophilic surface with a contact angle of 87.2°. Both oxidation processes produced similar properties in terms of corrosion behavior and showed better resistance than the as-received state in a certain range of potential. Moreover, the surface treatments led to no significant change in the protein adsorption levels, which indicates that the difference in viability between the osteoblast and fibroblast cells was not due to the difference in surface protein adsorption. Given all the factors, the surfaces obtained by anodic oxidation treatment revealed higher cell viability than those obtained by plasma oxidation ($p = 0.05$).

Keywords: Ti6Al4V; oxidation; corrosion; cell viability; protein adsorption

1. Introduction

Orthopedic implants are used for long bone fracture fixations, spinal fracture and deformity corrections and stabilizations, arthritic joint replacements, and maxillofacial applications. While these implants provide mechanical stability, they have to be biologically compatible with the implantation sites [1]. Various surface treatment techniques have been proposed to improve the biocompatibility, as well as the mechanical and electrochemical properties, of implant materials. These surface treatments can be performed for most of the metals used for implant manufacturing, such as titanium and its alloys. Titanium and its alloys have a certain degree of biocompatibility due to the natural passive oxide layer on their surfaces [2–3]. Although titanium alloys have high biocompatibility, alloying elements such as vanadium and aluminum can dissolve after implantation and are then released into the tissue, causing poor osseointegration. While vanadium ions are particularly cytotoxic, aluminum ions are suspected to induce neurological diseases [4–5]. Passive films formed on the surfaces of metallic implants slow down the corrosion reactions on the surface and reduce the dissolution rate of metals in the biological environment, thus prolonging the implants life. The surface oxide layers contribute to the adsorption of proteins and differentiation in bone cells. The thickness of these layers is also an important parameter for biocompatibility [6–7]. Anodic oxidation (anodization) is one of the surface treatments that can be used to create an oxide film as a result of reactions occurring on the surface of a metal workpiece attached to the system as a positive electrode in the electrolytic environment. The most important advantage of anodic oxidation is the strong bonding of oxides to the titanium surface [8]. Anodic oxidation is also applied to increase the corrosion resistance, to color the metal, and to create porous/rough surfaces by forming a thick oxide layer on the metal surface. The structural and chemical properties of the oxidized surfaces depend on process parameters such as potential, current, electrolyte composition, and temperature [9]. Another method employed to increase the fatigue strength, wear resistance, and corrosion resistance properties of metals is the glow discharge plasma oxidation. This method is a thermochemical process in which oxygen atoms are

Corresponding author: Özgü Bayrak E-mail: obayrak@erzincan.edu.tr

diffused to the material surface and form a hard layer on the surface in a gaseous plasma environment. Thermochemical treatments pose many advantages, such as a shorter treatment time, homogenous surface structures, the possibility of obtaining results similar to those of conventional methods at lower temperatures, less environmental impact and gas consumption, and more biocompatible materials [10–11]. The biocompatibility of implant materials is tested in a cell culture, which is an *in vitro* test system, prior to the clinical use of the materials. In this way, the use of experimental animals can be reduced. Recently, a wide range of studies on biocompatibility have been conducted, including those focusing on *in vitro* cytotoxicity and tissue-material interactions of materials [12–14]. Fibroblast cell lines are commonly used to test the cytotoxicity of implant materials, but these cell lines do not represent specific cells that are appropriate for bone tissues. Therefore, using fibroblast cells instead of osteoblast cells for bone tissues may cause incomplete interpretation to assess cytotoxicity [14]. The main goal of the current study is to determine whether fibroblast and osteoblast cell lines have different cell viabilities on the surface of Ti6Al4V alloy modified with anodic oxidation and glow discharge plasma oxidation techniques. Changes in the corrosion properties after the surface treatments were also investigated. The process parameters were selected based on factors such as scientific literature, industrial applicability, and plasma stability. Considering the plasma oxidation of pure or alloyed titanium, it has been reported that a diffusion layer that reaches saturation at low temperatures (400–500°C) is formed, but no significant oxide layer is formed. When the temperature is increased, the oxide layer is formed and thickens with further temperature increase, but the adhesion of this layer gradually decreases due to the tensile residual stresses in the material–oxide interface and high Pilling–Bedworth ratio [15–17]. Regarding the anodization, high voltages have been reported to have adverse effects on especially corrosion resistance, and at lower voltages, very thin layers form on the surface [18–20].

2. Experimental

2.1. Sample characterization and preparation

The chemical composition of the as-received alloy determined from energy-dispersive X-ray spectroscopy (EDS) analysis and the standard chemical composition given in the relevant standard are presented in Table 1.

Table 1. Chemical composition of Ti6Al4V alloy wt%

Alloy	Al	V	Fe	O	C	H	N	Ti	Others
ISO 5832-3	5.5–6.7	3.5–4.5	<0.30	<0.20	<0.08	<0.015	<0.05	87–91	<0.4
As-received	6.25	3.71	<0.30	<0.20	<0.08	<0.015	<0.05	Bal.	<0.4

Ti6Al4V alloy samples with a thickness of 3 mm were cut from a 14 mm diameter cylindrical bar. The surfaces of the samples were ground with 80, 220, 400, 600, 800, and 1200 silicon carbide emery papers to remove the undesirable surface layer affected by the heat of the cutting process and the resulting plastic deformation. The samples were cleaned in an acetone bath using an ultrasonic cleaner for 15 min and dried with hot air before surface treatments.

2.2. Anodic and glow discharge plasma oxidation

The anodic oxidation setup consisted of a direct-current power source (GPR-30H10D, 500 W, 50–60 Hz), a magnetic stirrer, a 400 mL beaker, and a magnetic fish to ensure the mixture homogeneity. Moreover, AISI type 304 stainless steel was used as the cathode, Ti6Al4V (grade 5) sample as the anode, and 1.5 mol/L H_2SO_4 (96% pure) as the solution. The sample holder was also manufactured from Ti6Al4V alloy. The process potential, duration, and temperature selected for the anodic oxidation process were 100 V, 10 min, and 25°C, respectively.

For glow discharge plasma treatment, the ground samples were cleaned with alcohol and dried with hot air. They were then placed on the 42CrMo4 alloy steel sample holder, which was also the system cathode. The chamber was vacuumed to 2.5 Pa. Prior to the surface treatment, preliminary sputtering was performed for 15 min under 500 V potential and H_2 atmosphere to remove possible contaminations from the samples. The chamber was re-vacuumed and filled with 100% pure O_2. The pressure was set to 500 Pa by a needle valve. The plasma environment was created via glow discharge as the direct current (DC) power supply was engaged. By adjusting the applied voltage, samples were heated up to the temperature determined according to the test plan. No additional heater was present in the plasma oxidation system. Since the samples were placed symmetrically on the sample holder, the temperature value of the sample in the middle was assumed to be the same for all samples. Plasma oxidation was carried out at 650°C for 1 h, and the samples were slowly cooled in a vacuum.

2.3. Surface characterization

2.3.1. Structural analysis

Structural analyses of the as-received and treated-surface samples were performed using X-ray diffraction (XRD, Panalytical Empyrean) and EDS. For the XRD measurements, Cu-Kα radiation with a wavelength of $\lambda = 15405.9$ nm was used, and the structures of the formed phases were determined by comparing the obtained diffraction patterns with

the International Center for Diffraction Data standard cards.

2.3.2. Surface and layer properties

Surface and cross-sectional images after both oxidation processes and corrosion tests were obtained using scanning electron microscopy (SEM, FEI Quanta EFG 450). For cross-sectional investigations, the top sides of the samples were ground and chemically etched with 10 mL HF (48wt%) + 90 mL H_2O for 5 min. The etched samples were rinsed with distilled water, cleaned in an ultrasonic cleaner, and dried with hot air. The surface roughness values before and after oxidation treatments were determined using atomic force microscopy (AFM, Park System XE-100-E).

Vickers microhardness measurements were carried out at the as-received and oxidized sample surfaces with a micro-Vickers hardness tester (Shimadzu HMV-G20D) at a constant load of 0.245 N and an indentation period of 15 s. At least five measurements, which would not affect one another, were performed for each sample and averaged.

2.3.3. Corrosion studies

Accelerated electrochemical tests were performed in triplicate under naturally stagnant condition using a potentiostat/galvanostat (Gamry Reference G750) in a 0.9wt% saline solution at 37 ± 1°C. The temperature was controlled by a thermostatic water bath. A conventional three-electrode system was adopted using saturated Ag/AgCl as the reference electrode and a graphite counter electrode. The measured sample with an exposed area of 0.38 cm^2 was utilized as the working electrode.

Open circuit potentials (OCPs) of the as-received and treated-surface samples were recorded continuously for 5400 s before cyclic polarization and electrochemical impedance spectroscopy (EIS) analyses. Forward scans of cyclic polarization tests were performed in the range of −250–1500 mV, referenced to the OCP, at a scanning rate of 1 $mV \cdot s^{-1}$. Reverse scans were performed until the OCP was reached. The EIS tests were performed using a frequency range of 0.1 Hz to 100 kHz under potentiostatic condition at OCP (0 mV vs. V_{OCP}) with a 10 mV amplitude alternating current (AC) voltage signal.

2.3.4. Contact angle

Static water contact angle measurements were carried out with an optical tensiometer (Attension Theta Lite) equipped with charge-coupled device (CCD) camera and light-emitting diode (LED) background illumination. The contact angles were determined by taking three measurements from different points on each sample using the sessile drop technique. Distilled water with a volume of 3.07 µL was used for measurements. After waiting 5 s for stabilization, recorded images of drops were automatically transferred to a computer, and the Young–Laplace model was used for contact angle estimation. Contact angles were measured from both sides of the sessile drop with automatic base line detection via computer software. The reported results are the arithmetic means of a total of six measurements for each sample.

2.4. Protein adsorption of Ti alloy surfaces

Tissue culture plates (TCPs) and the as-received and treated Ti6Al4V surfaces were sterilized under high pressure at 121°C for 20 min and then incubated with 500 µL of fetal bovine serum (FBS) (Sigma–Aldrich F7524) for 24, 48, and 72 h at 37°C in a humidified 5vol% CO_2 atmosphere. When the incubation time was completed, samples were removed and rinsed twice with phosphate buffer solution (Sigma–Aldrich P3619). Adsorbed proteins on the samples were detached into 500 µL of 5wt% sodium dodecyl sulfate (SDS, Sigma–Aldrich #436143) solution by shaking for 15 min. The protein amounts in the SDS solutions were measured via Bradford assay (Pierce Coomassie Protein Assay Kit #23200). The optical density values of the solutions were determined at 562 nm in a spectrophotometer (iMark, Bio-Rad).

2.5. Cell lines culture

Mouse fibroblast cell lines (L929) and human osteoblast (hFOB) cell lines were cultured in a DMEM/F12 medium (Sigma–Aldrich D9785), which was supplemented with 10vol% FBS, 100 IU/mL of penicillin, and 100 µg/mL of streptomycin solution (Gibco PenStrep #15140-122). The culture was carried out at 37°C temperature in a humidified 5vol% CO_2 atmosphere. The medium was renewed every three days. The cells were then passaged when they reached confluence. Furthermore, 0.25vol% trypsin/Ethylenediaminetetraacetic acid (EDTA) (Pan Biotech #P10-019500) solution was used to detach the cells. The cells were counted in a hemocytometer and plated at a density of 4×10^4 cells/well on 24-well TCPs, sterilized as-received Ti6Al4V (control), and treated Ti alloy surfaces. The plates were incubated for 24, 48, and 72 h to assess the cell viability assay.

The colorimetric assay MTT (3-(4,5-dimethythiazol-2-yl)-2,5-diphenyl tetrazolium bromide) (Serva #20395) was used to determine the cell viability after 24, 48, and 72 h of incubation on TCPs and Ti alloy samples. Yellow MTT was reduced to insoluble dark purple formazan via mitochondrial succinate dehydrogenase. Since only living cells can participate in this reaction, the level of reduced MTT is accepted as a scale of cell viability. The cells were incubated at 37°C for 3 h after 50 µL/well of MTT solution was added. After incubation, dimethylsulfoxide (Sigma–Aldrich #472301) was added to each well to dissolve the color. Lastly, a microplate reader was used to determine the absorbance values, since the optical absorbance values of the MTT are directly proportional to the number of viable cells.

2.6. Statistics

Experiments were performed in triplicate. Values were expressed as mean ± standard deviation (SD). The SPSS 16.0

software was used for statistical analysis. The absorbance values of each group were first normalized, and then, a one-way ANOVA test was performed to find significant differences between groups. For the groups that were different, Tukey's test was performed to determine statistically significant differences. The significance level was less than 5% ($p \leq 0.05$).

3. Results

3.1. Crystal structure analyses

The XRD patterns of as-received and treated-surface samples are given in Fig. 1. As expected, the as-received Ti6Al4V samples consisted of hexagonal closed pack alpha and body-centered cubic beta phases, since Ti6Al4V is a metastable α+β alloy. After the plasma oxidation process, rutile-TiO_2, which is the most stable polymorph of titania, was formed on the surface. However, in the case of anodic oxidation, the dominant TiO_2 phase was found to be anatase, which is a metastable polymorph of titania. Some small diffractions of rutile were also observed.

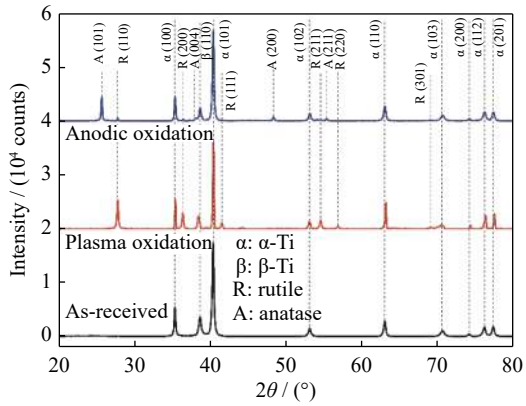

Fig. 1. X-ray diffraction patterns of Ti6Al4V alloy before and after plasma oxidation and anodic oxidation.

3.2. Surface and layer properties

Fig. 2 shows the SEM images of the surfaces of samples treated by plasma oxidation and anodic oxidation. The oxide layer obtained from plasma oxidation (Fig. 2(a)) exhibited a fairly homogenous and dense structure, while anodic oxidation yielded a more porous oxide layer (Fig. 2(b)). The average diameter of pores was measured as ~170 nm. In the plasma oxidation process, the oxygen plasma spread uniformly to the surface, and a homogeneous surface was formed because of the low temperature and short processing time, which resulted in the limited sputtering of Ti ions from the surface and subsequent re-condensation on the surface. Therefore, the surface topography from the previous surface finish was evident in the SEM image. The chemical compositions (wt%) of the plasma oxidation- and anodic oxidation-treated surfaces are given in Table 2.

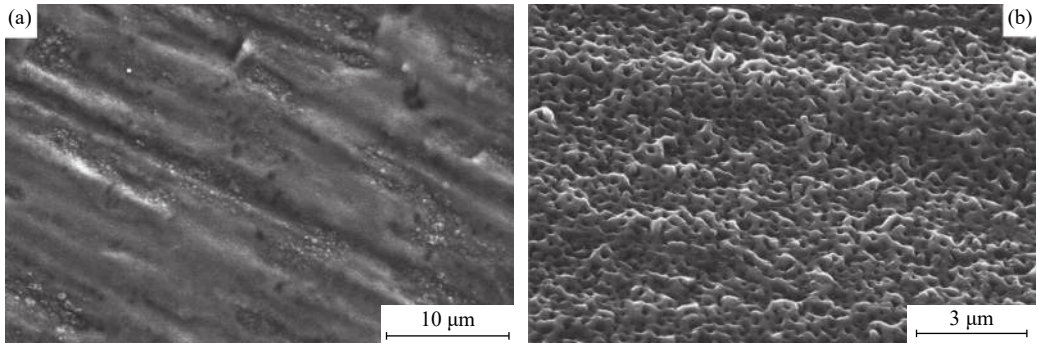

Fig. 2. SEM images of (a) plasma-oxidized and (b) anodically oxidized surfaces.

Table 2. Chemical compositions of plasma oxidation- and anodic oxidation-treated surfaces wt%

Sample	Ti	Al	V	O	Others
Plasma oxidation-treated surface	40.00	0.58	0.90	58.30	0.22
Anodic oxidation-treated surface	41.55	0.42	0.69	57.22	0.12

The AFM images of the as-received, plasma-oxidized, and anodically oxidized samples (Fig. 3) provide results similar to those derived from the SEM images. Based on the AFM images, the average surface roughness values (R_a) were determined as ~200, ~220, and ~130 nm for the as-received, plasma-oxidized, and anodically oxidized samples, respectively.

Fig. 4 presents the microhardness and roughness values of the surfaces. Both oxidation processes resulted in increase in the surface hardness. The increase in hardness was around 118% for plasma oxidation and around 35% for anodic oxidation.

Figs. 5(a) and 5(b) show the cross-sectional microstructures after plasma oxidation and anodic oxidation. The aver-

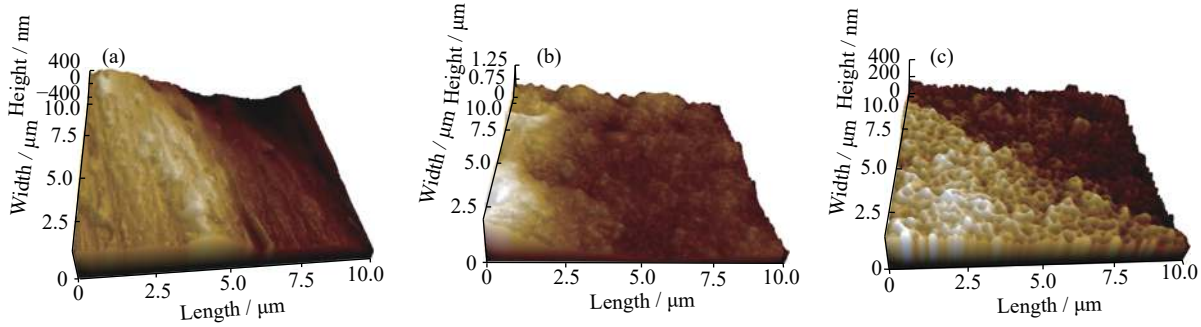

Fig. 3. AFM images of (a) as-received, (b) plasma-oxidized, and (c) anodically oxidized surfaces.

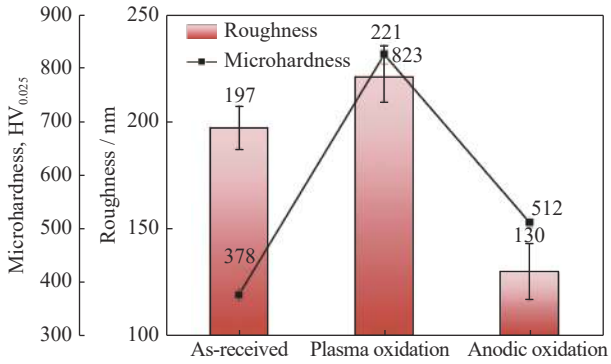

Fig. 4. Surface roughness (R_a) and surface microhardness of Ti6Al4V alloy before and after oxidations.

age oxide layer thickness values were measured as 1.2 and 0.95 μm for the plasma-oxidized and anodically oxidized samples, respectively. The oxide layers were observed to be separated from the surfaces, which is due to the chemical etching procedure applied to obtain a better contrast between the layer and the base material.

3.3. Contact angle

Contact angle water drop profiles are presented in Fig. 6. Both oxidation processes created less hydrophilic surfaces. While the contact angle of the as-received sample was 49.35°, plasma oxidation yielded a surface with a contact angle of 74.92°. Anodic oxidation, on the other hand, produced the least hydrophilic surface, with a contact angle of 87.20°.

3.4. Corrosion studies

Fig. 7(a) shows the OCP graphs of the as-received and ox-

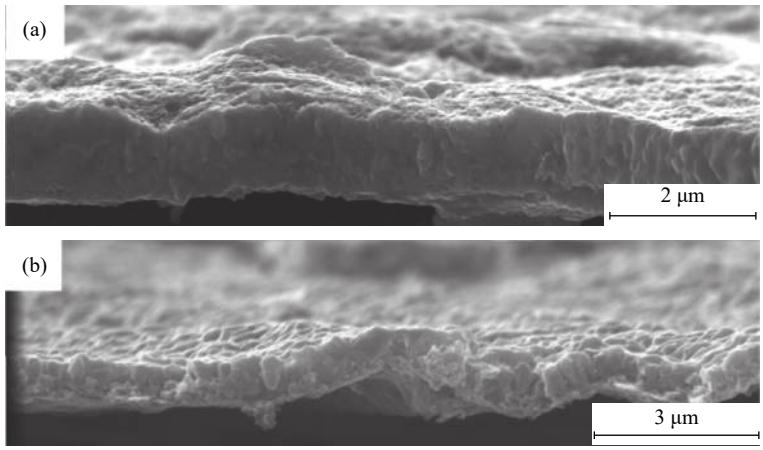

Fig. 5. Microstructure of samples of Ti6Al4V in cross section after (a) plasma oxidation and (b) anodic oxidation.

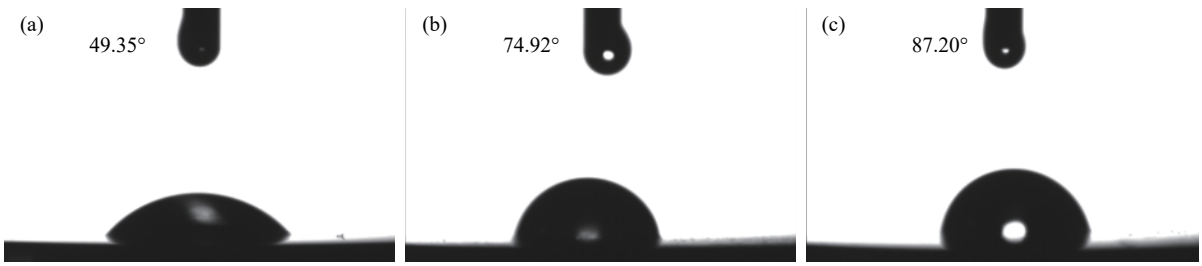

Fig. 6. Water drop profiles of (a) as-received, (b) plasma-oxidized, and (c) anodically oxidized surfaces.

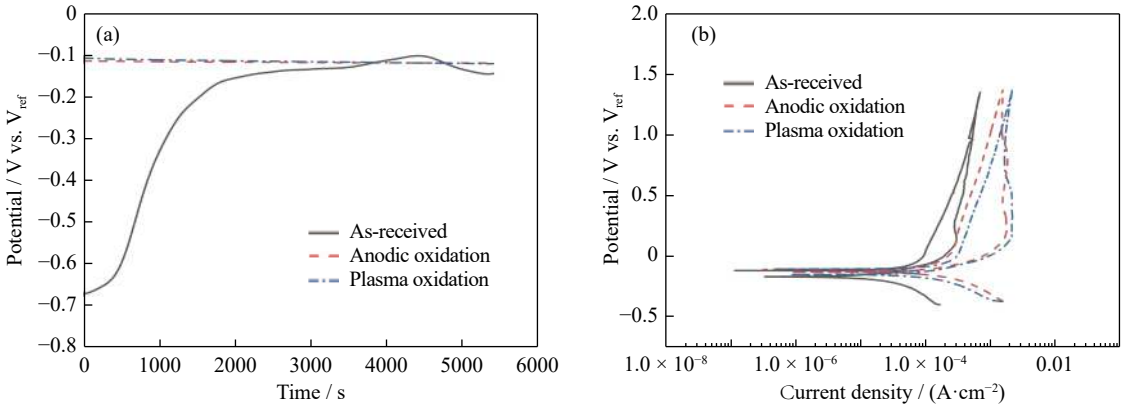

Fig. 7. Open circuit potential (a) and cyclic polarization curves (b) of as-received and oxidized samples.

idized samples. Open circuit potential, or free potential, is the potential of any freely immersed electrode in an environment. Based on the principle of charge conservation, the accumulation of charge on a freely immersed electrode should be avoided. This can only be achieved if the sum of the oxidation currents is equal to the sum of the reduction currents. The as-received Ti6Al4V sample had a very low potential as it was first immersed into the solution, but its potential climbed toward the positive direction over time. The OCPs of both anodically and plasma-oxidized samples were similar from the beginning of the test. All three samples reached a steady state between −0.1 and −0.15 V vs. V_{ref} (V_{ref} is the potential of reference electrode Ag/AgCl).

Cyclic polarization curves of the untreated and treated samples in saline solution are given in Fig. 7(b). The as-received surface exhibited a very limited passivity in the anodic region between 0.15 and 0.25 V. Anodic dissolution occurred after this potential region was passed, and it continued until the forward scan was complete. Both oxidized samples showed a pronounced stable passive state right after the Tafel region. In the case of plasma oxidation, anodic dissolution started again after approximately −1 V. The reverse scan current densities were lower than the forward scan current densities for all three samples. Only the as-received sample yielded repassivation potential (E_{rp}) during the reverse scan.

Quantitative values obtained from the Tafel region are provided in Table 3. The free corrosion potentials of both treated samples were positively shifted. On the other hand, the corrosion current density of the untreated sample was lower than those of the oxidized samples; therefore, the corrosion rate of the untreated sample, which was calculated based on Faraday's law, was slightly lower than those of the treated samples. Considering that the calculated corrosion rate was solely based on the quantitative values of the Tafel region and did not represent the entire polarization range, weight loss was also measured and is given in Table 3.

Table 3. Results obtained from Tafel extrapolations and weight measurements

Sample	I_{corr} / (A·cm^{-2})	E_{corr} / mV	β_A / (V·dec^{-1})	β_C / (V·dec^{-1})	Corrosion rate / (mm·a^{-1})	Weight loss / wt%
As-received	$1.25 \times 10^{-4} \pm 2.18 \times 10^{-6}$	−147 ± 5.3	0.447 ± 0.0399	0.860 ± 0.0243	2.019 ± 0.035	0.225 ± 0.025
Anodic oxidation	$2.07 \times 10^{-4} \pm 6.55 \times 10^{-6}$	−120 ± 2.5	0.283 ± 0.0210	0.336 ± 0.0279	2.12 ± 0.067	0.159 ± 0.019
Plasma oxidation	$2.48 \times 10^{-4} \pm 2.47 \times 10^{-5}$	−129 ± 2.6	0.254 ± 0.0221	0.231 ± 0.0276	2.55 ± 0.25	0.718 ± 0.087

Note: I_{corr}, E_{corr}, β_A, and β_C denote corrosion current desnity, corrosion potential, anodic slope, and cathodic slope, respectively.

Complex plane (Nyquist) plots of untreated and treated samples obtained from EIS measurements and a diagram of the equivalent electrical circuit used for data interpretation are shown in Fig. 8. All three conditions yielded similar ohmic resistances (R_u), which represent the resistances of the solution, wires, and connections and other uncompensated resistances [21]. The as-received sample exhibited a single time constant system. The diameter of the semi-circle, which represents the polarization or charge transfer resistance, was considerably wide. After plasma oxidation and anodic oxidation treatments, the samples yielded at least two noticeable time constants. The first time constant at the high-frequency region represents coating, and those for both treated samples featured similar attributes. At middle and low frequencies, mass transport (diffusion) seemed to play a role and created a more complicated mixed control case at the oxidized samples. The electron exchange rate between the active species in solution and sample surface became very high; the corrosion rate was controlled by the diffusion of corrosion products toward or away from the test electrode, which appears as a nearly straight line with a slope of approximately 45°. Therefore, a Warburg impedance (W_d) was added to the corresponding equivalent circuit model, which also consisted of a capacitor and a resistor, creating an equivalent circuit with mixed kinetic and charge transfer control [22]. The Warburg impedance is dependent on the perturbation fre-

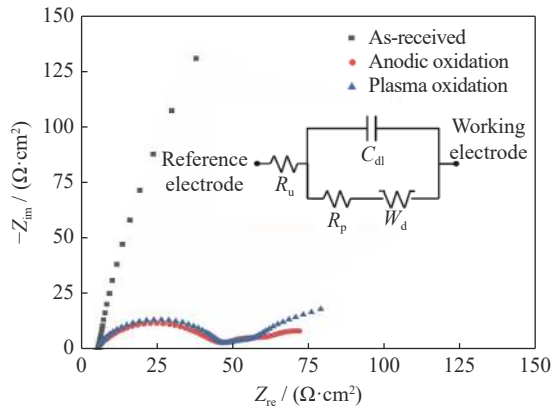

Fig. 8. Nyquist graph and equivalent electrical circuit of as-received and oxidized samples. Z_{re} is the real part of impedance (resistance), and Z_{im} is the imaginary part of impedance (reactance).

quency, and it has a small value at high frequencies because reactants move short distances. At low frequencies, on the other hand, the diffusing reactants have to move farther, which in return increases the Warburg impedance. The capacitor element C_{dl} in the circuit model represents the capacitance of the electrical double layer that forms at the electrode surface. The resistor R_p denotes the charge transfer resistance of the electrical double layer. Even though the as-received sample exhibited only kinetic control and could be represented by a simple equivalent electrical circuit such as the Randles circuit, the mixed control circuit including Warburg impedance was also used for this sample in order to compare the results. The quantitative results of circuit elements are given in Table 4.

Fig. 9 shows the SEM micrographs of the as-received and oxidized samples after polarization tests. The as-received state (Fig. 9(a)) exhibited severe deterioration, evidenced by the small pits and spalling observed at the surface. The anodic-oxidation sample showed almost no sign of corrosion (Fig. 9(b)). This result agrees with the polarization graphs. The plasma-oxidation sample exhibited some cracks and pits at the surface, resembling blistering (Fig. 9(c)).

3.5. Protein adsorption and cell viability on surfaces

After Ti6Al4V surface modifications, the results of protein adsorption and cell viability were obtained to analyze the effect of the modifications. As shown in Fig. 10(a), the protein adsorption levels on all surfaces were similar for all time points ($p \geq 0.05$). The surface treatments had no significant effect on the protein adsorption of surfaces.

As seen in Fig. 10(b), the fibroblast cell viabilities on surfaces specially produced for cell cultures at all time points were statistically higher than those for other surfaces (as-received, plasma-treated, and anodization-treated) ($p \leq 0.05$). The fibroblast cell viabilities on as-received and plasma-treated surfaces were similar at 24 and 48 h, whereas that in the anodization-treated surfaces was higher ($p \leq 0.05$). At the

Table 4. Quantitative results of circuit elements

Sample	R_u / (Ω·cm²)	C_{dl} / (μF·cm^{-2})	W_d / (S·s$^{1/2}$·cm^{-2})	R_p / (Ω·cm²)
As-received	6.931 ± 0.039	19.34 ± (<0.01)	0.0027 ± 0.00007	1602 ± 11.75
Anodic oxidation	7.065 ± 0.002	1.61 ± (<0.01)	0.09 ± 0.0019	37.78 ± 0.206
Plasma oxidation	7.672 ± 0.003	1.03 ± (<0.01)	0.11 ± 0.0026	35.41 ± 0.213

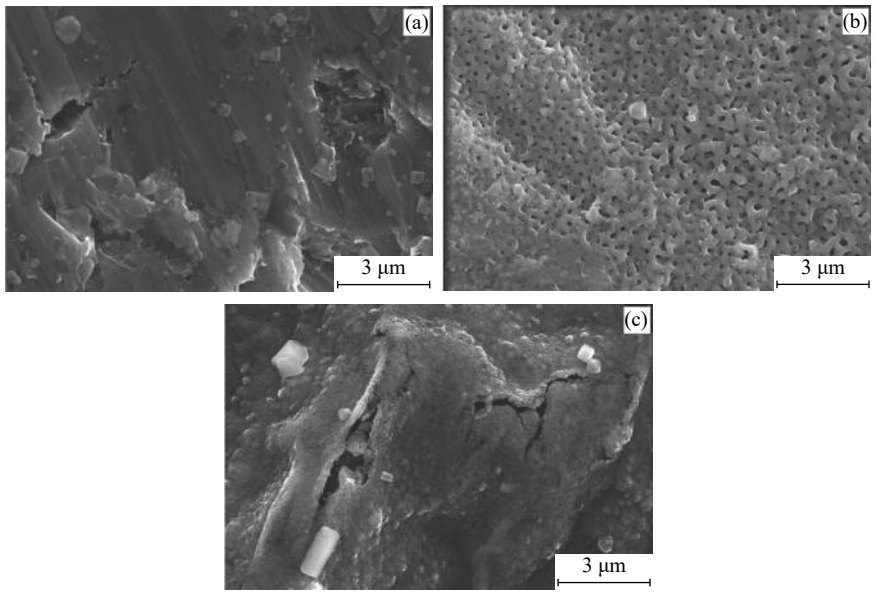

Fig. 9. Surface SEM images after polarization: (a) as-received; (b) anodic-oxidation; (c) plasma-oxidation samples.

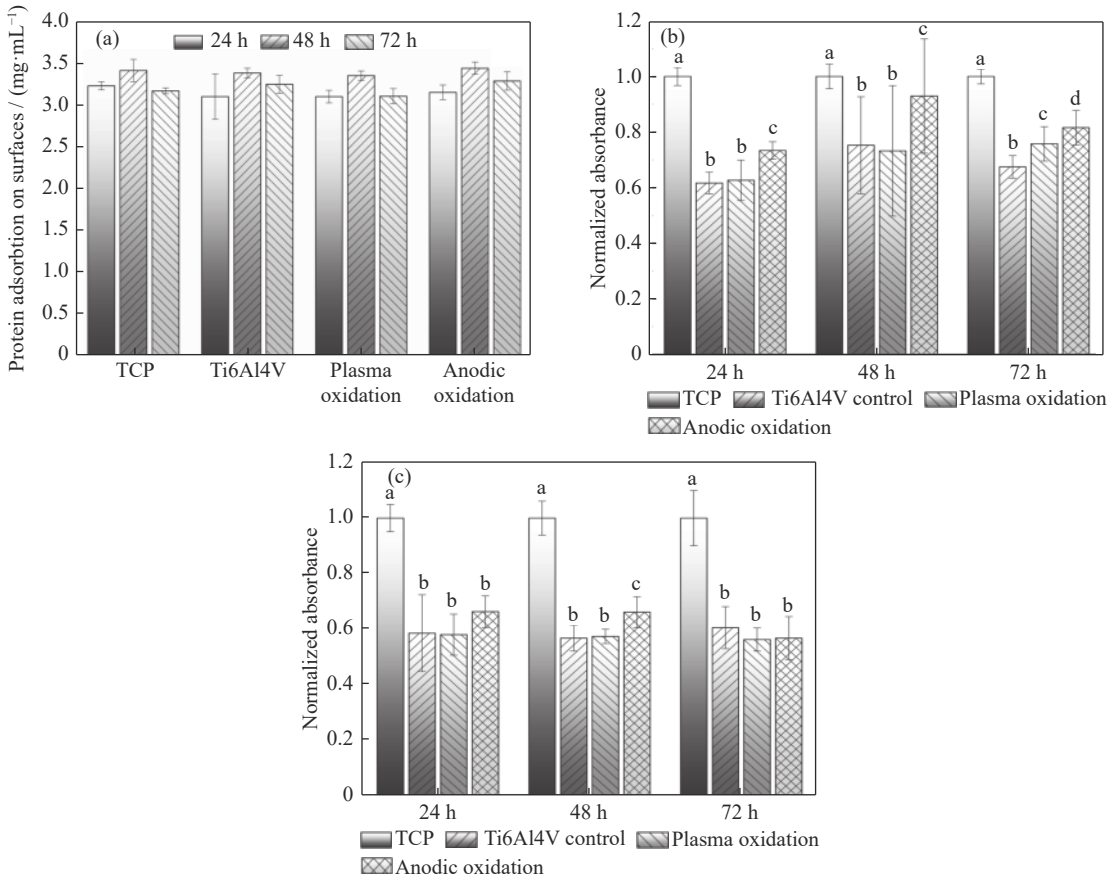

Fig. 10. Protein adsorption of surfaces (a), fibroblast cell viability (b), and osteoblast cell viability (c) on TCP and Ti6Al4V surfaces before and after oxidation. a, b, c, and d show statistically significant differences between variables.

end of 72 h, the fibroblast cell viability on the plasma-treated surfaces was found to be higher than that on the as-received Ti6Al4V surfaces (as-received surfaces) ($p \leq 0.05$). In the figure, the bars with different letters are significantly different at the 0.05 level.

The viability of osteoblast cells, as well as fibroblast cells, on the TCP surfaces was highest for all time durations compared with those on other surfaces ($p \leq 0.05$) (Fig. 10(c)). The osteoblast cell viabilities on all TiAl4V surfaces were statistically similar for 24 and 72 h ($p \geq 0.05$), while the cell viability on the anodization-treated surfaces was slightly higher than that on the plasma-treated surfaces for 48 h ($p \leq 0.05$), Although a more detailed study is required, the surface properties are believed to be unnoticeable for osteoblast cells compared with fibroblast cells.

4. Discussion

In accordance with the XRD results, the glow discharge plasma oxidation procedure yielded an oxide layer dominated by rutile-TiO_2. Since the plasma oxidation procedure was performed under vacuum conditions, rutile formation at a relatively lower temperature was facilitated. Anodic oxidation was performed under ambient pressure and temperature. Therefore, the oxide layer consisted of anatase-TiO_2 phase. Some minor diffractions from rutile phase were also evident and are known to be formed after a certain anodic oxidation period [23], at around 100 V potential [24]. Diffractions belonging to the substrate metal on the oxidized surfaces indicate relatively thin oxide layers, which are also evident at cross-sectional SEM micrographs.

The obtained EDS results prove that oxide layers with similar chemical compositions were formed on the surface, which was expected since both anatase and rutile phases have the same TiO_2 stoichiometry and tetragonal crystallographic structure but different lattice parameters. The EDS results also revealed that the alloying elements Al and V occurred in a negligible quantity at the surface area. This result is analogous with the findings of Satoh *et al.* [25] and was reported to be caused by the local depletion of such elements, which have possible toxic effects, from the outermost surface.

The AFM analyses indicated that the plasma oxidation process increased the surface roughness due to the ion and electron bombardment that occurred during the procedure. Particles with high kinetic energy in the plasma environment impact on the surface, causing the sputtering of atoms, ions, or electrons from the surface [26–28].

In the anodic oxidation process, however, a nanoporous

surface emerged, due to abrupt electrical discharges. Since the sample was the anode of the oxidation system, surface asperities were subjected to anodic dissolution due to the higher current density of such peak points [29]. The formed oxide layer also filled up the roughness valleys. Hence, the surface topography generated by the prior mechanical surface finish seemed to be less pronounced.

The surface hardness values were high on both oxidized surfaces compared with the as-received state. Both anatase and rutile phases are oxide ceramics and exhibit high resistance to local deformation. Bulk rutile is known to be harder than bulk anatase due to the crystal structure of the former. In addition, the diffusion layer formed underneath the oxide layer during plasma oxidation increased the load-bearing capacity of the surface in our case. Since this study is focused on cell response on the surfaces, the sub-surface structure was not analyzed.

The as-received sample exhibiting varying OCPs during immersion in saline solution indicates that an electrochemically unstable surface was present. The ascending nature of the curve coincides with the decrease in the anodic reaction rate due to the formation of a natural oxide surface film. On the other hand, the occurrence of almost constant potential values of oxidized samples throughout the test suggests that chemically stable/noble surfaces were achieved with both surface treatment procedures [30–32].

The lower current densities on reverse scan indicate negative hysteresis, and negative hysteresis is usually associated with a passive surface film, which is capable of repairing itself. This situation was observed for all three samples. Within the three test conditions, only the as-received surface displayed repassivation potential (E_{rp}) during the reverse scan, which is indicative of a chemically less stable surface.

Despite the corrosion rate calculation results, the sample exposed to anodic oxidation had the lowest weight loss, and the untreated sample had the highest weight loss. While the anodic-oxidation sample showed strong passivation during polarization, the as-received sample was exposed to anodic dissolution that continued throughout the experiment.

As mentioned before, all three samples exhibited very similar ohmic resistance values, which was expected since the tests were performed at virtually the same conditions. The double-layer capacitor and polarization resistance values of the as-received sample were higher by orders of magnitude than those of the oxidized samples. The Warburg impedance of the untreated sample was so small that it was negligible and thus has no real physical equivalent in this sample. It can be concluded that under free potential conditions, the as-received state can store more charge and resist better than the oxidized states. Warburg impedance showed that the diffusion was very similar in the oxidized samples; that is, a similar diffusion process occurred.

Because the as-received sample did not exhibit passivation and dissolved continuously during polarization, the surface of this sample showed pitting and spalling. The surface of the anodic-oxidation sample remained intact after the polarization measurements. The strong passivation exhibited by this sample protected the surface against anodic dissolution. Delamination, which was observed on the surface of the plasma-treated sample, seemed to originate from under the oxide layer and may be caused by the diffusion of corrosion products and reactants from the surface, changing the course of corrosion reaction from the surface to oxide layer interface.

Contact angle measurements indicated that the anodized alloy surface was less hydrophilic than the surfaces of the other samples, but the difference between two oxide surfaces was not considerable. Proteins tend to adhere more to hydrophobic surfaces than to hydrophilic surfaces [33]; however, in this study, no statistically significant differences were observed for protein adsorption among the three investigated Ti6Al4V surfaces. The higher contact angle of the anodically oxidized surface is attributed to the nanoporous structure. Moreover, since rutile phase has a greater chemical stability than anatase, the free energy of anatase-dominant surface was believed to be higher [34].

The interaction of an implant and its surrounding is influenced by various factors, including implant surface topology. Surfaces with a wide variety of properties such as topology, chemistry, or roughness can be achieved via several preparation methods [35]. Even though cell reaction is influenced by the combined effect of several factors, it has been reported that rougher surfaces may enhance adhesion, proliferation, and vitality [35–37]. It is also expected that surface treatments lead to more cell proliferation by causing more protein adsorption, especially for bone implants [38]. However, in the present study, we noticed that cell proliferation was independent of protein adsorption because the as-received surface and oxidized surfaces had similar protein levels.

The fibroblast cells were shown to exhibit a higher affinity for anodic oxidation-treated Ti6Al4V surfaces with a nanoporous topography rather than plasma-treated surfaces with a non-porous structure. As the anodization process created a porous structure and a titanium oxide layer with an anatase phase on the implant surface, this method yielded more cell viability for both cell lines compared with the glow discharge plasma oxidation. As mentioned by Crespo *et al.* [39], surface texture and composition may influence cell anchorage and therefore cell proliferation. However, the optimal surface properties have not yet been clearly defined for the attachment, proliferation, and differentiation of cells [38].

Surface treatments may lead to different levels of ion release from the Ti6Al4V surface, and especially, the osteoblast cells may be more susceptible to this ion release level [40]. Additionally, no differences were observed between cells cultured on the untreated or treated alloy in some previ-

ous studies. Therefore, we can conclude that cell proliferation on biomaterial is not a rule. Activities, morphologies, and differentiation of cells may also be affected [39]. On the other hand, even if the treated alloy can show better biocompatibility, attention should be paid to signs of inflammation as reported by Chen *et al.* [41]. We demonstrated that no significant changes in osteoblast cell viability were observed among the investigated surfaces, which agrees with the finding of Silva *et al.* [42]. Therefore, we may conclude that the osteoblast cells had less viability than the fibroblasts on treated surfaces.

In vitro biocompatibility studies that show the cellular response of titanium alloys after different surface treatments have been conducted using osteoblastic cells (mouse MC3T3-E1) [43–45], fibroblast [45–46], rat bone marrow cells and human umbilical vein endothelial cells [47–48], osteosarcoma cells [49], normal epithelial cells [50], and human peripheral blood mononuclear cells [48,51]. In most biomaterial cytotoxicity analyses, fibroblast cells are used. However, fibroblast cells and tumor-derived cells do not represent the normal bone cells and tissues [14]. Moreover, determining cell viability is not enough to decide the biocompatibility of a material; therefore, the cell spreading, differentiation, and inflammation caused by the biomaterial should also be determined.

5. Conclusion

The effects of anodic and plasma oxidation processes on the corrosion properties and the cell response of Ti6Al4V alloy were investigated. As a result of the anodic oxidation process, a nanoporous anatase-TiO_2 surface with an average pore diameter of ~170 nm was formed. The plasma oxidation process, on the other hand, yielded a non-porous and relatively dense rutile-TiO_2 structure. The surface roughness of the sample after plasma oxidation (~220 nm) was slightly greater than that of the as-received condition (~200 nm). The anodic oxidation process caused the surface roughness to decrease to ~130 nm. Both oxidation processes produced layers with high hardness. The rutile-dominant surface obtained by plasma oxidation exhibited a much higher hardness, with an increase of 118% compared with the as-received condition. With the anodic oxidation process, a 35% increase was achieved. The thicknesses of the formed layers were similar for the plasma oxidation and anodic oxidation processes and measured around 1 μm. Hydrophilicity was lowest on the anodization-treated surface, with a contact angle of 87.2°. The OCP measurements showed that the oxidized surfaces demonstrated similar corrosion behaviors and were more electrochemically stable than the as-received sample. Moreover, while Tafel extrapolations indicated that the corrosion of the as-received sample was lower than those the oxidized surfaces, polarization and weight loss measurements showed that the oxidized surfaces exhibited passivation. The anodically oxidized sample presented the highest corrosion resistance. The EIS studies also revealed that the corrosion reactions on the oxidized surfaces were carried out by complex mechanisms, including mass transfer (diffusion). The protein adsorption levels on the surfaces were found to be similar for all samples after the 24-, 48-, and 72-h periods. Fibroblast cell viability was higher in the anodized sample than in the untreated sample. The plasma-treated surface and the as-received surface exhibited similar viabilities after the 24- and 48-h periods, while the former exhibited a higher viability after the 72-h period. Similarly, the anodized surface featured a better osteoblast cell viability after 48 h. Lastly, although measuring cell viability may offer an idea to determine the biomaterial compatibility, differentiation, migration, gene expressions, and antibacterial effects should be evaluated for a more accurate determination.

Acknowledgements

This work was financially supported by Erzincan Binali Yıldırım University Research Fund (No. FBA-2018-547). Authors acknowledge Prof. Dr. Bora Garipcan for enabling the authors to Biomaterials Laboratory of Biomedical Engineering Institute, Boğaziçi University and Prof. Dr. Ayhan Çelik for permitting the use of glow discharge plasma oxidation at Mechanical Engineering Laboratory in Ataturk University.

References

[1] S.B. Goodman, Z.Y. Yao, M. Keeney, and F. Yang, The future of biologic coatings for orthopaedic implants, *Biomaterials*, 34(2013), No. 13, p. 3174.

[2] C. Oldani and A. Dominguez, Titanium as a biomaterial for implants, [in] S. Fokter, ed., *Recent Advances in Arthroplasty*, InTechOpen, London, 2012, p. 149.

[3] M. Saini, Y. Singh, P. Arora, V. Arora, and K. Jain, Implant biomaterials: A comprehensive review, *World J. Clin. Cases*, 3(2015), No. 1, p. 52.

[4] K. Wang, The use of titanium for medical applications in the USA, *Mater. Sci. Eng. A*, 213(1996), No. 1-2, p. 134.

[5] A. Zieliński, S. Sobieszczyk, T. Seramak, W. Serbiński, B. Świeczko-Żurek, and A. Ossowska, Biocompatibility and bioactivity of load-bearing metallic implants, *Adv. Mater. Sci.*, 10(2010), No. 4, p. 21.

[6] A.F. Yetim, F. Yildiz, Y. Vangolu, A. Alsaran, and A. Celik, Several plasma diffusion processes for improving wear properties of Ti6Al4V alloy, *Wear*, 267(2009), No. 12, p. 2179.

[7] P. Stratton and M. Graf, Wear of diffusion hardened Ti–6Al–4V sliding against tool steel, *Wear*, 268(2010), No. 3-4, p. 612.

[8] X.Y. Liu, P.K. Chu, and C.X. Ding, Surface modification of titanium, titanium alloys, and related materials for biomedical applications, *Mater. Sci. Eng. R*, 47(2004), No. 3-4, p. 49.

[9] S. Minagar, C.C. Berndt, J. Wang, E. Ivanova, and C.E. Wen, A review of the application of anodization for the fabrication of nanotubes on metal implant surfaces, *Acta Biomater.*, 8(2012),

No. 8, p. 2875.
[10] B.E. Rapuano, H. Singh, A.L. Boskey, S.B. Doty, and D.E. MacDonald, Heat and radiofrequency plasma glow discharge pretreatment of a titanium alloy: Eveidence for enhanced osteoinductive properties, *J. Cell. Biochem.*, 114(2013), No. 8, p. 1917.
[11] D.E. MacDonald, B.E. Rapuano, P. Vyas, J.M. Lane, K. Meyers, and T. Wright, Heat and radiofrequency plasma glow discharge pretreatment of a titanium alloy promote bone formation and osseointegration, *J. Cell. Biochem.*, 114(2013), No. 10, p. 2363.
[12] K.L. Anderson, E.E. Apolinario, S.R. MacAuley, and K.R. Sowers, A 5' leader sequence regulates expression of methanosarcinal CO dehydrogenase/acetyl coenzyme A synthase, *J. Bacteriol.*, 191(2009), No. 22, p. 7123.
[13] A. Pizzoferrato, G. Ciapetti, S. Stea, E. Cenni, C.R. Arciola, and D. Granchi, Cell culture methods for testing biocompatibility, *Clin. Mater.*, 15(1994), No. 3, p. 173.
[14] J.M. Anderson, Future challenges in the *in vitro* and *in vivo* evaluation of biomaterial biocompatibility, *Regen. Biomater.*, 3(2016), No. 2, p. 73.
[15] M. Rinner, J. Gerlach, and W. Ensinger, Formation of titanium oxide films on titanium and Ti6Al4V by O_2-plasma immersion ion implantation, *Surf. Coat. Technol.*, 132(2000), No. 2-3, p. 111.
[16] M.A.M. Silva, A.E. Martinelli, C. Alves, R.M. Nascimento, M.P. Távora, and C.D. Vilar, Surface modification of Ti implants by plasma oxidation in hollow cathode discharge, *Surf. Coat. Technol.*, 200(2006), No. 8, p. 2618.
[17] F. Borgioli, E. Galvanetto, F.P. Galliano, and T. Bacci, Air treatment of pure titanium by furnace and glow-discharge processes, *Surf. Coat. Technol.*, 141(2001), No. 1, p. 103.
[18] S. Uttiya, D. Contarino, S. Prandi, M.M. Carnasciali, G. Gemme, L. Mattera, R. Rolandi, M. Canepa, and O. Cavalleri, Anodic oxidation of titanium in sulphuric acid and phosphoric acid electrolytes, *J. Mater. Sci. Nanotechnol.*, 1(2014), No. 1, p. S106.
[19] W. Asumpinwong, K. Saengkiettiyut, and V. Srimaneepong, Different constant voltages of anodization on the corrosion behavior of Ti–6Al–4V alloy, *Chiang Mai J. Sci.*, 42(2015), No. 1, p. 239.
[20] A.K. Sharma, Anodizing titanium for space applications, *Thin Solid Films*, 208(1992), No. 1, p. 48.
[21] A. Lasia, Electrochemical impedance spectroscopy and its applications, [in] B.E. Conway, J.O. Bockris, and R.E.White, eds., *Modern Aspects of Electrochemistry*, Springer, Boston, 2002.
[22] H.A. Acciari, D.P.S. Palma, E.N. Codaro, Q.Y. Zhou, J.P. Wang, Y.H. Ling, J.Z. Zhang, and Z.J. Zhang, Surface modifications by both anodic oxidation and ion beam implantation on electropolished titanium substrates, *Appl. Surf. Sci.*, 487(2019), p. 1111.
[23] H.D. Traid, M.L. Vera, A.E. Ares, and M.I. Litter, Porous titanium dioxide coatings obtained by anodic oxidation for photocatalytic applications, *Procedia Mater. Sci.*, 9(2015), p. 619.
[24] T.A. Soares, H. Mozaffari, and H. Reinecke, Generation of microstructures on a Ti–6Al–4V substrate through anodization, *Surf. Coat. Technol.*, 278(2015), p. 64.
[25] K. Satoh, S. Sato, and K. Wagatsuma, Formation mechanism of toxic-element-free oxide layer on Ti–6Al–4V alloy in d.c. glow discharge plasma with pure oxygen gas, *Surf. Coat. Technol.*, 302(2016), p. 82.
[26] A. Çelik, M. Aslan, A.F. Yetim, and Ö. Bayrak, Wear behavior of plasma oxidized CoCrMo alloy under dry and simulated body fluid conditions, *J. Bionic Eng.*, 11(2014), No. 2, p. 303.
[27] M. Aslan, O. Çomaklı, M. Yazıcı, A.F. Yetim, Ö. Bayrak, and A. Çelik, The effect of plasma oxidation and nitridation on corrosion behavior of CoCrMo alloy in SBF solution, *Surf. Rev. Lett.*, 25(2018), No. 08, art. No. 1950024.
[28] A. Çelik, Ö. Bayrak, A. Alsaran, İ. Kaymaz, and A.F. Yetim, Effects of plasma nitriding on mechanical and tribological properties of CoCrMo alloy, *Surf. Coat. Technol.*, 202(2008), No. 11, p. 2433.
[29] A. Yli-Pentti, Electroplating and electroless plating, [in] S. Hashmi, G.F. Batalha, C.J.V. Tyne, and B. Yilbas, eds., *Comprehensive Materials Processing*, Elsevier, 2014.
[30] A.C. Alves, F. Wenger, P. Ponthiaux, J.P. Celis, A.M. Pinto, L.A. Rocha, and J.C.S. Fernandes, Corrosion mechanisms in titanium oxide-based films produced by anodic treatment, *Electrochim. Acta*, 234(2017), p. 16.
[31] D. Veys-Renaux, Z.A.E. Haj, and E. Rocca, Corrosion resistance in artificial saliva of titanium anodized by plasma electrolytic oxidation in Na_3PO_4, *Surf. Coat. Technol.*, 285(2016), p. 214.
[32] K. Elagli, M. Traisnel, and H.F. Hildebrand, Electrochemical behaviour of titanium and dental alloys in artificial saliva, *Electrochim. Acta*, 38(1993), No. 13, p. 1769.
[33] K.Y. Cai, J. Bossert, and K.D. Jandt, Does the nanometre scale topography of titanium influence protein adsorption and cell proliferation?, *Colloids Surf. B*, 49(2006), No. 2, p. 136.
[34] B.E. Li, J. Li, C.Y. Liang, H.P. Li, L.T. Guo, S.M. Liu, and H.S. Wang, Surface roughness and hydrophilicity of titanium after anodic oxidation, *Rare Met. Mater. Eng.*, 45(2016), No. 4, p. 858.
[35] M. Lukaszewska-Kuska, P. Wirstlein, R. Majchrowski, and B. Dorocka-Bobkowska, Osteoblastic cell behaviour on modified titanium surfaces, *Micron*, 105(2018), p. 55.
[36] A. Wennerberg and T. Albrektsson, Effects of titanium surface topography on bone integration: A systematic review, *Clin. Oral Implan. Res.*, 20(2009), No. s4, p. 172.
[37] M. Bachle and R.J. Kohal, A systematic review of the influence of different titanium surfaces on proliferation, differentiation and protein synthesis of osteoblast-like MG63 cells, *Clin. Oral Implan. Res.*, 15(2004), No. 6, p. 683.
[38] L.L. Guehennec, M.A. Lopez-Heredia, B. Enkel, P. Weiss, Y. Amouriq, and P. Layrolle, Osteoblastic cell behaviour on different titanium implant surfaces, *Acta Biomater.*, 4(2008), No. 3, p. 535.
[39] L. Crespo, M. Hierro-Oliva, S. Barriuso, V. Vadillo-Rodríguez, M.Á. Montealegre, L. Saldaña, E. Gomez-Barrena, J.L. González-Carrasco, M.L. González-Martín, and N. Vilaboa, On the interactions of human bone cells with Ti6Al4V thermally oxidized by means of laser shock processing, *Biomed. Mater.*, 11(2016), No. 1, art. No. 015009.
[40] C.H. Ku, D.P. Pioletti, M. Browne, and P.J. Gregson, Effect of different Ti–6Al–4V surface treatments on osteoblasts behaviour, *Biomaterials*, 23(2002), No. 6, p. 1447.
[41] J. Chen, S. Mwenifumbo, C. Langhammer, J.P. McGovern, M. Li, A. Beye, and W.O. Soboyejo, Cell/surface interactions and adhesion on Ti–6Al–4V: Effects of surface texture, *J. Biomed. Mater. Res. Part B*, 82(2007), No. 2, p. 360.
[42] W. de Melo Silva, C.A. Ribeiro, C.S. Marques, A.S. Tabata, M.J. Saeki, L.I. Medeiros, and D.E. de Oliveira, Fibroblast and pre-osteoblast cell adhesive behavior on titanium alloy coated with diamond film, *Mater. Res.*, 20(2017), No. suppl 2, p. 284.
[43] Y. Shibata and Y. Tanimoto, A review of improved fixation methods for dental implants Part I: Surface optimization for

rapid osseointegration, *J. Prosthodont. Res.*, 59(2015), No. 1, p. 20.

[44] J.H. Park, R. Olivares-Navarrete, R.E. Baier, A.E. Meyer, R. Tannenbaum, B.D. Boyan, and Z. Schwartz, Effect of cleaning and sterilization on titanium implant surface properties and cellular response, *Acta Biomater.*, 8(2012), No. 5, p. 1966.

[45] E. Czarnowska, A. Sowinska, B. Cukrowska, J.R. Sobiecki, and T. Wierzchoń, Response of human osteoblast-like cells and fibroblasts to titanium alloy nitrided under glow discharge conditions, *Mater. Sci. Forum*, 475-479(2005), p. 2415.

[46] E. Czarnowska, T. Wierzchoń, and A. Maranda-Niedbała, Properties of the surface layers on titanium alloy and their biocompatibility in *in vitro* tests, *J. Mater. Process. Technol.*, 92-93(1999), p. 190.

[47] S. Bruni, M. Martinesi, M. Stio, C. Treves, T. Bacci, and F. Borgioli, Effects of surface treatment of Ti–6A1–4V titanium alloy on biocompatibility in cultured human umbilical vein endothelial cells, *Acta Biomater.*, 1(2005), No. 2, p. 223.

[48] C. Treves, M. Martinesi, M. Stio, A. Gutiérrez, J.A. Jiménez, and M.F. López, *In vitro* biocompatibility evaluation of surface-modified titanium alloys, *J. Biomed. Mater. Res. Part A*, 92(2010), No. 4, p. 1623.

[49] C.F. Huang, H.C. Cheng, C.M. Liu, C.C. Chen, and K.L. Ou, Microstructure and phase transition of biocompatible titanium oxide film on titanium by plasma discharging, *J. Alloys Compd.*, 476(2009), No. 1-2, p. 683.

[50] A. El-Ghannam, L. Starr, and J. Jones, Laminin-5 coating enhances epithelial cell attachment, spreading, and hemidesmosome assembly on Ti–6Al–4V implant material *in vitro*, *J. Biomed. Mater. Res.*, 41(1998), No. 1, p. 30.

[51] M. Martinesi, S. Bruni, M. Stio, C. Treves, and F. Borgioli, *In vitro* interaction between surface-treated Ti–6Al–4V titanium alloy and human peripheral blood mononuclear cells, *J. Biomed. Mater. Res. Part A*, 74(2005), No. 2, p. 197.